第 42 卷 第 5 期
2021 年 5 月

焊 接 学 报
TRANSACTIONS OF THE CHINA WELDING INSTITUTION

Vol. 42(5):45 − 50
May 2021

高压干法 X65 管线钢 GMAW 焊接接头在模拟海水中的腐蚀行为

张忠明[1,2]， 薛龙[2]， 李齐龙[1]， 黄继强[2]， 徐春杰[1]
(1. 西安理工大学, 西安, 710048; 2. 北京石油化工学院, 光机电装备技术北京市重点实验室, 北京, 102617)

摘要: 高压干法熔化极气体保护焊 (简称 GMAW) 在海底油气管道等水下构件的组装和维修中有着非常广泛的应用, 焊接接头在海水中的腐蚀行为对于海底输油管道的安全运行至关重要. 通过模拟浸泡试验和极化曲线法研究不同环境压力下 (常压, 0.3 MPa, 0.5 MPa) X65 管线钢干法 GMAW 焊接接头在人工海水中的腐蚀行为及机理. 结果表明, 与焊缝和母材相比, 热影响区的耐蚀性最差, 且环境压力对焊接接头的腐蚀性能影响不明显. X65 管线钢干法 GMAW 焊接接头在人工海水中的腐蚀形式以点蚀为主, 在浸泡后期出现严重的局部腐蚀; 腐蚀产物由 FeOOH, Fe_2O_3, Fe_3O_4 组成, 腐蚀产物层在浸泡初期起到减缓金属腐蚀的作用, 但随着浸泡时间延长, 腐蚀产物层的致密性降低, 其下的金属接头容易遭受到 Cl^- 的破坏, 使局部腐蚀过程加剧.

创新点: (1) 阐明了干法 GMAW 焊接的 X65 管线钢焊接接头在人工海水中的腐蚀性能及腐蚀行为, 发现热影响区的耐蚀性最差, 焊接环境压力对焊接接头的腐蚀性能影响不大.

(2) 揭示了焊接接头的腐蚀机制, 腐蚀形式以点蚀为主, 明确了腐蚀产物的作用.

关键词: X65 管线钢; 高压焊接; 熔化极气体保护焊; 腐蚀性能

中图分类号: TG 444$^+$.72 **文献标识码:** A **doi:** 10.12073/j.hjxb.20200824001

0 序言

随着海洋油气的开发, 对石油管线性能的要求越来越高. 目前国内海底油气管线系统多采用具有良好抗拉强度、低温冲击韧度和可焊接性的 X65 级管线钢, 且大部分管道已经服役多年, 面临维护及更换问题[1-2], 水下焊接技术作为一种钢结构的主要连接方法, 在海洋管道的建设、日常维护及抢修中起着重要的作用, 而焊接接头良好的力学性能与耐腐蚀性能是保证海底油气管线系统安全工作的重要条件[3]. 常用的水下焊接方法有湿法焊接、干法焊接和局部干法水下焊接, 其中干法焊接又分为高压干法焊接和常压干法焊接两类[4]. 水下高压干法焊接质量好, 是快速、经济的管道维修方法之一[5]. 高压干法熔化极气体保护焊 (gas metal arcuwelding, 简称 GMAW) 具有焊接效率高、可进行全位置焊接、焊接稳定性好、易于实现焊接自动化等优势, 在海底油气管道、海上钻井平台等水下构件的组装和维修中有着非常广泛的应用[6-8]. 对于水下高压干法 GMAW 焊接的焊缝成形、焊缝组织及焊接接头的力学性能, 已有工作开展了相关研究. 李凯、刘剑和郑朋朋等人[6, 8-9] 研究了环境压力、焊接极性和焊接参数对水下高压干法 GMAW 焊缝成形的影响, 分析了焊接过程中主要参数与焊缝成形之间的关系. 冯静等人[10] 探索了湿度对高压环境下 GMAW 焊接质量与接头力学性能的影响规律. 刘宏、王瑜等人[11-12] 研究了环境压力对熔化极气体保护焊焊缝显微组织、硬度、强度及韧性的影响.

油气管线钢不仅要具有优异的力学性能, 还需要良好的耐腐蚀性能作为保证, 其服役环境是海水, 在海水中管线钢的腐蚀依赖于许多因素, 包括材料组成、pH 值、溶解氧含量、盐度、温度和流体速度等[13-14]. Vera 和刘智勇等人[15-16] 对管线钢在海水中的腐蚀行为进行了研究, 发现在海水腐蚀中钢表面会生成腐蚀产物膜, 并指出点蚀是其主要的腐蚀形式. 孔德军等人[17] 对管线钢焊接接头的腐蚀

收稿日期: 2020 − 08 − 24

基金项目: 国家自然科学基金资助项目 (51275051); 北京市自然科学基金—北京市教委联合资助项目 (KZ20180017022); 光机电装备技术北京市重点实验室开放课题 (KF2013-01).

研究表明，覆盖在试样表面的腐蚀产物膜在达到一定厚度后，能够阻隔试样与腐蚀介质的接触，有利于抑制腐蚀的持续进行. 范舟等人[18] 的研究表明，在海水中管线钢焊接接头不同区域的电极电位不同，且在腐蚀过程中会发生变化. 刘智勇和林鑫等人[19-20] 对钢的焊接件在海水中的腐蚀行为进行了研究，发现在焊接接头的 3 个区域中热影响区的腐蚀电位最负，这会引发焊缝与热影响区之间的电偶腐蚀. 这些研究都对管线钢在海水中的腐蚀行为进行了探讨，但对于水下高压干法 GMAW 焊接的 X65 钢焊接接头的腐蚀性能还缺乏相关的研究. 开展不同环境压力下 X65 钢焊接接头的腐蚀行为特别是在海水中的腐蚀行为非常必要，可为海底输油管道工程建设安装和安全运行提供技术支持.

1 试验方法

试验所用的 API X65 管线钢与 JM-68 焊丝的化学成分如表 1. 利用高压焊接试验系统通过模拟水下常压 (0.1 MPa) 和高压 (0.3 和 0.5 MPa) 干法 GMAW 焊接得到焊接接头[6, 12]. 腐蚀介质为人工海水 (pH 值 7.7)，其化学成分 (g/L) 为 NaCl 24.53, $MgCl_2$ 5.20, $NaSO_4$ 4.09, $CaCl_2$ 1.16, KCl 0.695, $NaHCO_3$ 0.201, KBr 0.101, H_3BO_3 0.027, $SrCl_2$ 0.025, NaF 0.003. 人工海水溶液采用分析纯化学试剂和蒸馏水进行配制. 根据 JB/T 7901—2001《金属材料实验室均匀腐蚀全浸试验方法》，试验溶液的用量为每平方厘米的试样表面积不少于 20 mL.

表 1 焊接母材及焊丝的化学成分 (质量分数，%)

Table 1 Chemical compositions of welding base metal and welding wire

材料	C	Si	Mn	P	S	Cr	Ni	Ti	Cu	Fe
X65 管线钢	0.07	0.28	1.19	0.006	0.01	0.25	0.04	—	0.10	余量
JM-68焊丝	0.08	0.08	1.76	0.014	0.03	—	—	0.09	—	余量

浸泡试验采用 30 mm × 20 mm × 3 mm 的片状挂片试样，焊缝位于试样中部，每组采用 3 个平行试样，试样表面用砂纸逐级打磨至 2000 号，用乙醇清洗后吹干待用. 浸泡周期分别为 15 天、30 天和 60 天，每 7 天更换一次溶液. 对腐蚀产物进行收集并使用 XRD 分析腐蚀产物相组成. 浸泡结束后，将试样浸入除锈液 (500 mL 浓盐酸 + 500 mL 去离子水 + 3.5 g 六次甲基四铵) 中超声清洗，烘干后进行 SEM 腐蚀形貌观察.

对焊接接头不同区域进行取样. 母材、焊缝和热影响区的取样尺寸相同，均为 10 mm × 10 mm × 3 mm，其中 10 mm × 10 mm 面作为工作面. 在工作面的背面点焊引出 Cu 导线，非工作面用环氧树脂包封. 工作面用砂纸逐级打磨至 2000 号，用乙醇清洗后吹干待用. 采用三电极体系，在 CS310 电化学工作站上进行电化学测试，试样为工作电极，铂片电极为辅助电极，饱和甘汞电极 (SCE) 为参比电极. 动电位极化曲线扫描范围为相对于开路电位 −0.5 ~ 1 V，扫描速率为 1 mV/s.

2 试验结果与讨论

2.1 极化曲线

图 1 为不同环境压力下焊接接头母材、焊缝和热影响区 3 个区域的动电位极化曲线. 可以看出，不同环境压力下焊接接头的自腐蚀电位变化规律相同，都是焊缝的自腐蚀电位最正，母材次之，而热影响区的最负. 从阳极极化曲线可以看出，各个曲线在−0.8 ~ −1.0 V 附近开始出现电位的强烈正移，电流密度随电位的增大变化微小，这表明 3 种焊接压力下焊接接头不同区域处的极化曲线都出现了钝化区间，说明在极化过程中，工作电极表面形成了钝化膜，这使得耐腐蚀性能有所提高[21-22]. 当电位过高时，钝化膜被击穿破坏，阳极溶解过程继续进行. 腐蚀电流密度 I_c 和极化电阻 R_p 可以用来表征金属的耐腐蚀能力[23]. 使用 CorrView 数据分析软件对图 1 的极化曲线进行拟合，得到不同环境压力下焊接接头不同区域的腐蚀电流密度和极化电阻，结果如表 2 所示.

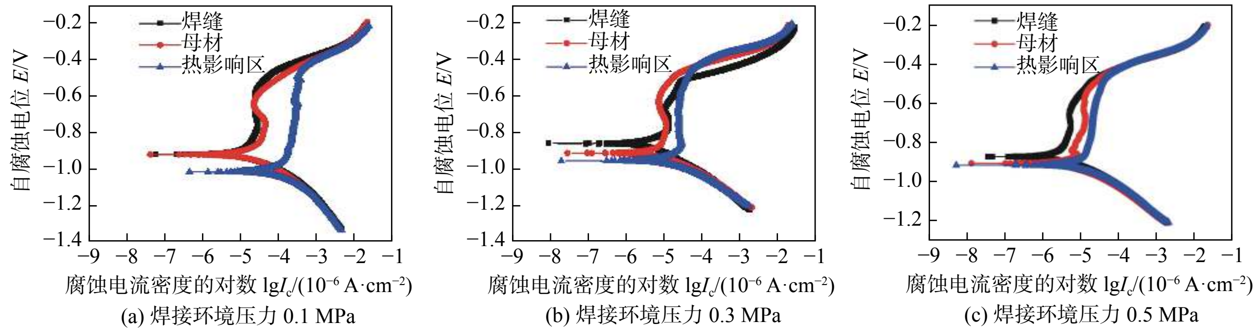

图 1　不同环境压力下焊接接头不同区域的动电位极化曲线

Fig. 1　Polarization curves of different zones of welded joints under different ambient pressures. (a) 0.1 MPa; (b) 0.3 MPa; (c) 0.5 MPa

表 2　极化曲线数据拟合

Table 2　Fitting data of polarization curve

区域	焊接环境压力0.1 MPa		焊接环境压力0.3 MPa		焊接环境压力0.5 MPa	
	腐蚀电流密度 $I_c/(10^{-6}\mathrm{A\cdot cm^{-2}})$	电极电阻 $R_p/(\Omega\cdot\mathrm{cm^{-2}})$	腐蚀电流密度 $I_c/(10^{-6}\mathrm{A\cdot cm^{-2}})$	电极电阻 $R_p/(\Omega\cdot\mathrm{cm^{-2}})$	腐蚀电流密度 $I_c/(10^{-6}\mathrm{A\cdot cm^{-2}})$	电极电阻 $R_p/(\Omega\cdot\mathrm{cm^{-2}})$
焊缝	4.1	2 437	4.7	2 394	4.8	2 321
母材	6.1	2 269	6.3	2 289	7.3	2 260
热影响区	15.5	1 649	10.7	1 888	14.3	1 518

常压焊接时, 焊缝、母材和热影响区的极化电阻分别是 2 437, 2 269 和 1 649 Ω/cm^2. 从热力学的角度来说, 自腐蚀电位和极化电阻越小, 说明腐蚀反应越易进行. 腐蚀电流密度是指工作电极表面单位面积上通过的电流大小, 反映了腐蚀的动力学, 更能说明腐蚀反应进行的程度和腐蚀速率. 常压下, 焊缝的腐蚀电流密度最小 (4.1×10^{-6} A/cm^2), 而热影响区的腐蚀电流密度最大 (1.5×10^{-5} A/cm^2), 热影响区的腐蚀电流密度较焊缝的腐蚀电流密度高出 3 倍多. 说明常压焊接环境下, X65 管线钢焊接接头不同区域的腐蚀速率由高到低依次为热影响区、母材和焊缝. 0.3 和 0.5 MPa 焊接环境压力下焊接接头不同区域的极化电阻与自腐蚀电流密度变化规律与常压焊接时相同, 均是焊缝的耐腐蚀性能最高, 热影响区的耐腐蚀性能最差.

仔细对比表 2 中不同环境压力下焊接接头的腐蚀电流密度和极化电阻, 发现焊接接头不同区域的腐蚀电流密度和极化电阻无明显差别, 这说明在试验范围内, 环境压力对 X65 管线钢干法 GMAW 焊接接头的腐蚀性能的影响可以不予考虑.

2.2　腐蚀形貌

图 2 为 3 种焊接环境压力下的焊接接头分别浸泡 15 天、30 天和 60 天后的腐蚀形貌. 可以看到, 浸泡 15 天的试样表面出现了均匀腐蚀和轻微的点蚀, 且 3 个焊接压力下的试样腐蚀差异不大; 浸泡 30 天后有尺寸较大的点蚀坑出现, 但是数量不多; 浸泡 60 天后, 浸泡前期产生的点蚀坑腐蚀加重, 试样出现了严重的局部腐蚀. 通过对比腐蚀形貌, 可以观察到 3 种焊接环境压力下的焊接接头的腐蚀形式主要为点蚀. 浸泡中期在试样表面观察到腐蚀产物层, 这对腐蚀有一定的减缓作用; 浸泡后期观察到腐蚀产物层剥落, 使得试样表面重新暴露在腐蚀溶液中, 后期腐蚀程度进一步加深, 有严重的局部腐蚀产生.

由于腐蚀液中存在 Cl^-, 它在金属表面有很强的吸附能力, 其吸附能力比氧更强, 因此 Cl^- 优先吸附在金属表面. 在点蚀坑的形成初期阶段, 氯离子通过腐蚀液向阳极点迁移, 导致在点蚀坑附近的氯化物浓度增高, 并从金属表面把氧排挤掉, 且氯化物和金属反应的速度较快, 形成了不稳定的可溶性物质, 这种反应使点蚀加速[24], 从而使得腐蚀产物剥落后金属的腐蚀加剧.

2.3　腐蚀产物

图 3 为不同焊接压力下的焊接接头在人工海水中浸泡 60 天后腐蚀产物的 XRD 图. 可以看出经过较长时间的浸泡后, 3 种焊接环境压力下的焊接接头在人工海水中的腐蚀产物组成相同, 均含有 FeOOH, Fe_2O_3 和 Fe_3O_4.

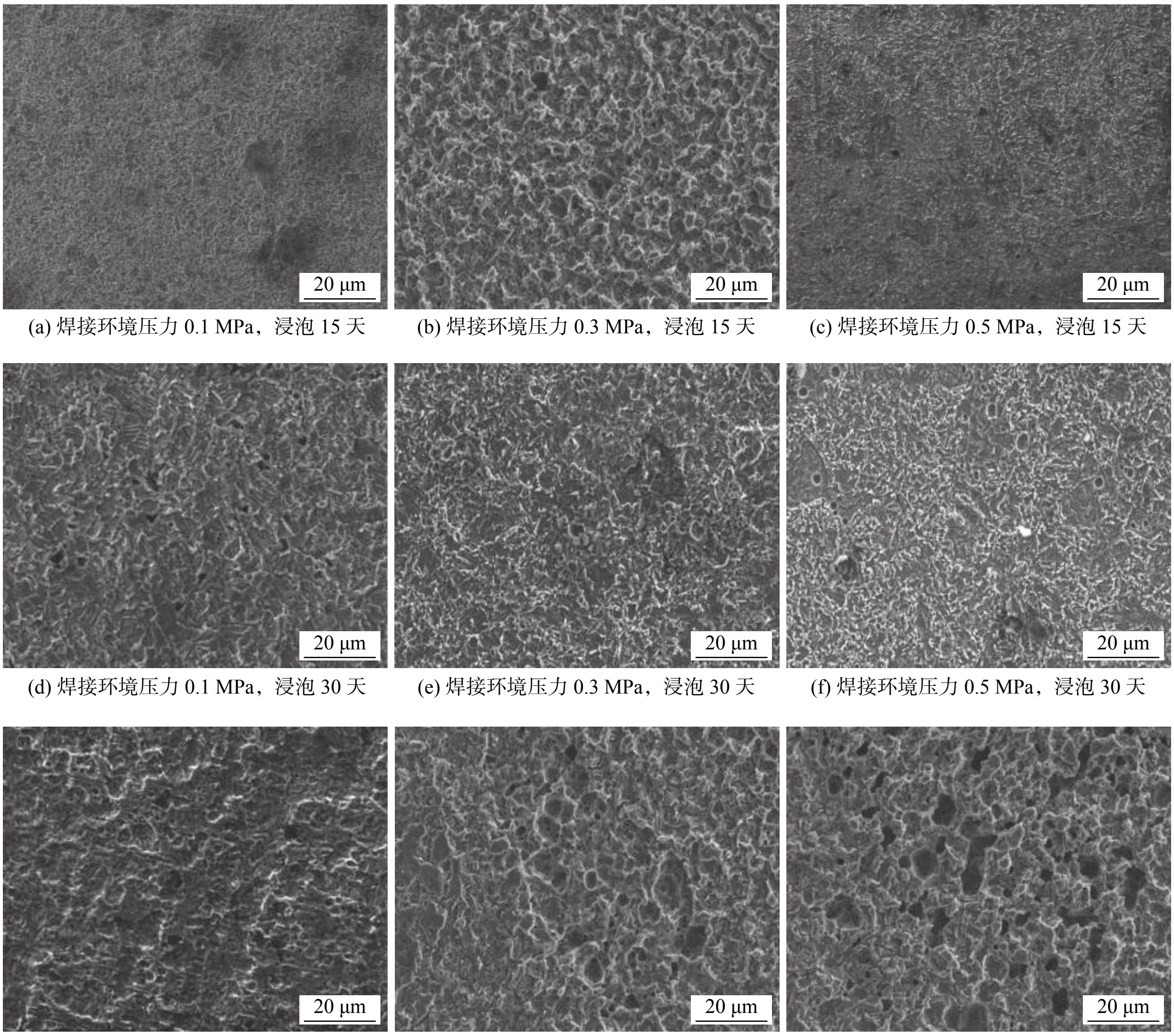

(a) 焊接环境压力 0.1 MPa，浸泡 15 天　(b) 焊接环境压力 0.3 MPa，浸泡 15 天　(c) 焊接环境压力 0.5 MPa，浸泡 15 天

(d) 焊接环境压力 0.1 MPa，浸泡 30 天　(e) 焊接环境压力 0.3 MPa，浸泡 30 天　(f) 焊接环境压力 0.5 MPa，浸泡 30 天

(g) 焊接环境压力 0.1 MPa，浸泡 60 天　(h) 焊接环境压力 0.3 MPa，浸泡 60 天　(i) 焊接环境压力 0.5 MPa，浸泡 60 天

图 2　浸泡不同时间后各个环境压力下的焊接接头的微观形貌

Fig. 2　SEM images of corrosion morphology of welded joints under different ambient pressures after immersion for different periods in simulated seawater. (a) 0.1 MPa, 15 days; (b) 0.3 MPa, 15 days; (c) 0.5 MPa, 15 days; (d) 0.1 MPa, 30 days; (e) 0.3 MPa, 30 days; (f) 0.5 MPa, 30 days; (g) 0.1 MPa, 60 days; (h) 0.3 MPa, 60 days; (i) 0.5 MPa, 60 days

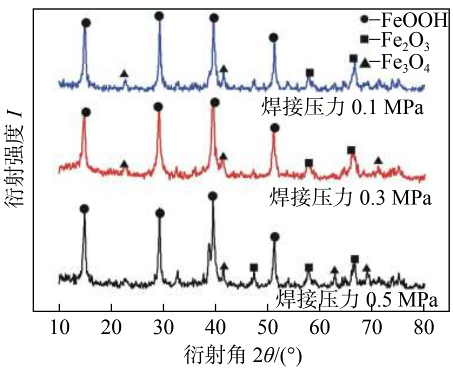

图 3　3 种焊接压力焊接接头浸泡 60 天腐蚀产物 XRD 图谱

Fig. 3　XRD spectrum of the collected corrosion products of the welded joints under different ambient pressures for 60 days of immersion in simulated seawater

由于腐蚀试验用人工海水置于大气环境中，空气中的 O_2 会充分溶入人工海水中，使得人工海水中的氧含量与空气中的氧分压相平衡. X65 管线钢焊接接头在人工海水中的腐蚀反应可以表示如下.

阴极反应 (O_2 的去极化过程)

$$O_2 + 2H_2O + 4e \rightarrow 4OH^- \tag{1}$$

阳极反应 (铁的氧化过程)

$$Fe - 2e \rightarrow Fe^{2+} \tag{2}$$

$$Fe^{2+} + 2OH^- = Fe(OH)_2 \tag{3}$$

电极反应形成的腐蚀产物 $Fe(OH)_2$ 附着在金属表面. 由于人工海水富氧，生成的 $Fe(OH)_2$ 会进一步氧化脱水，形成具有一定保护性的腐蚀产物层 (如 γ-FeOOH).

$$Fe(OH)_2 + O_2 \rightarrow Fe_3O_4或FeOOH \tag{4}$$

Fe 的氧化物形成水合物时体积会增大,产生的腐蚀产物层并不致密. 在 Cl^-的作用下,腐蚀产物层的保护性容易受到破坏[25],在腐蚀产物层下形成闭塞腐蚀区域而发生点蚀,导致在焊接接头形成了较多的点蚀坑 (图 2). 同时,Fe 作为反应的阳极被氧化后与溶液中的 OH-以及 O_2 结合生成了铁的氧化物.

$$4Fe(OH)_2 + O_2 + 2H_2O = 4Fe(OH)_3 \tag{5}$$

$$2Fe(OH)_3 + nH_2O = Fe_2O_3 \cdot nH_2O + 3H_2O \tag{6}$$

可见,在人工海水中 X65 管线钢焊接接头腐蚀反应的腐蚀产物主要由 FeOOH, Fe_2O_3 和 Fe_3O_4 组成.

3　结论

(1) 在常压的人工海水工况下,焊接环境压力对高压干法 X65 管线钢 GMAW 焊接接头腐蚀性能影响不明显. 焊接接头不同区域的耐蚀性由高到低依次为焊缝、母材和热影响区.

(2) X65 管线钢焊接接头在人工海水中腐蚀形式主要为点蚀. 浸泡后期腐蚀程度进一步加深,有严重的局部腐蚀产生.

(3) X65 管线钢焊接接头在人工海水中的腐蚀产物主要由 FeOOH, Fe_2O_3 和 Fe_3O_4 组成,对焊接接头表面有一定的保护作用. 随着浸泡时间延长,腐蚀产物层破坏剥落,致使后期腐蚀加剧.

参考文献

[1] 周建龙, 李晓刚, 程学群, 等. 深海环境下金属及合金材料腐蚀研究进展 [J]. 腐蚀科学与防护技术, 2010, 22(1): 47 − 51.
Zhou Jianlong, Li Xiaogang, Cheng Xuequn, *et al*. Research progress on corrosion of metallic materials in deep sea environment[J]. Corrosion Science & Protection Technology, 2010, 22(1): 47 − 51.

[2] 丁扬. X65 管线钢高压 GMAW 工艺研究 [D]. 哈尔滨: 哈尔滨工业大学, 2014.
Ding Yang. Research on X65 pipeline steel GMAW process under high pressure[D]. Harbin: Harbin Institute of Technology, 2014.

[3] Majumdar J D. Underwater welding-present status and future scope[J]. Journal of Naval Architecture and Marine Engineering, 2006, 3(1): 38 − 47.

[4] Łabanowski J, Fydrych D, Rogalski G. Underwater welding-a review[J]. Advances in Materials Science, 2009, 8(3): 11 − 22.

[5] 黄继强, 薛龙, 吕涛, 等. 水下高压空气环境下 GMAW 电弧特性试验 [J]. 焊接学报, 2010, 31(12): 17 − 20.
Huang Jiqiang, Xue Long, Lü Tao, *et al*. Experiment on characteristics of GMAW arc in underwater hyperbaric air condition[J]. Transactions of the China Welding Institution, 2010, 31(12): 17 − 20.

[6] 刘剑, 薛龙, 黄继强, 等. 水下高压干式环境下压力及焊接参数对 GMAW 焊缝成形的影响 [J]. 焊接学报, 2016, 37(2): 29 − 32.
Liu Jian, Xue Long, Huang Jiqiang, *et al*. Effect of pressure and welding parameters on weld bead geometry of GMAW in underwater hyperbaric dry environment[J]. Transactions of the China Welding Institution, 2016, 37(2): 29 − 32.

[7] Xue Long, Wu Jinming, Huang Junfen, *et al*. Welding polarity effects on weld spatters and bead geometry of hyperbaric dry GMAW[J]. Chinese Journal of Mechanical Engineering, 2016, 29(2): 351 − 356.

[8] 郑朋朋, 薛龙, 黄继强, 等. 基于多因素权重法的高压 GMAW 焊缝成形分析 [J]. 焊接学报, 2018, 39(10): 75 − 80.
Zheng Pengpeng, Xue Long, Huang Jiqiang, *et al*. Analysis on weld bead geometry of hyperbaric GMAW based on multi-factor weighting method[J]. Transactions of the China Welding Institution, 2018, 39(10): 75 − 80.

[9] 李凯, 高洪明, 李海超, 等. 焊接极性对水下高压干法 GMAW 影响分析 [J]. 焊接学报, 2014, 35(8): 108 − 112.
Li Kai, Gao Hongming, Li Haichao, *et al*. Effect of welding polar on dry hyperbaric GMAW process[J]. Transactions of the China Welding Institution, 2014, 35(8): 108 − 112.

[10] 冯静, 薛龙, 黄军芬, 等. 高压环境下湿度对低碳钢熔化极气体保护焊焊接质量的影响 [J]. 上海交通大学学报, 2016, 50(10): 1631 − 1634.
Feng Jing, Xue Long, Huang Junfen, *et al*. Influence of humidity on welding quality of gas metal arc welding in hyperbaric environment[J]. Journal of Shanghai Jiao Tong University, 2016, 50(10): 1631 − 1634.

[11] 刘宏, 薛龙, 黄继强, 等. 环境压力对熔化极气体保护焊焊缝强度及韧性的影响 [J]. 上海交通大学学报, 2016, 50(10): 1613 − 1617.
Liu Hong, Xue Long, Huang Jiqiang, *et al*. Influence of environmental pressure on strength and toughness of weld by Gas Metal Arc Welding[J]. Journal of Shanghai Jiao Tong University, 2016, 50(10): 1613 − 1617.

[12] 王瑜, 黄继强, 薛龙, 等. 不同环境压力下 X65 管线钢焊接接头的组织及硬度 [J]. 铸造技术, 2016, 37(10): 2193 − 2196.
Wang Yu, Hang Jiqiang, Xue Long, *et al*. Microstructure and hardness of welding joints of X65 pipeline steel under different environmental pressures[J]. Foundry Technology, 2016, 37(10): 2193 − 2196.

[13] Igor A Chaves, Robert E Melchers. Pitting corrosion in pipeline

steel weld zones[J]. Corrosion Science, 2011, 53(12): 4026 − 4032.

[14] Rihan R O. Electrochemical corrosion behavior of X52 and X60 steels in carbon dioxide containing saltwater solution[J]. Material Research, 2013, 16(1): 227 − 236.

[15] Vera R, Vinciguerra F, Bagnara M. Comparative study of the behavior of API 5L-X65 grade steel and ASTM A53-B grade steel against corrosion in seawater[J]. International Journal of Electrochemical Science, 2015, 10(8): 6187 − 6198.

[16] 刘智勇, 贾静焕, 杜翠薇, 等. X80 和 X52 钢在模拟海水环境中的腐蚀行为与规律 [J]. 中国腐蚀与防护学报, 2014, 34(4): 327 − 332.
Liu Zhiyong, Jia Jinghuan, Du Cuiwei, *et al*. Corrosion behavior of X80 and X52 steels in simulated seawater environments[J]. Journal of Chinese Society for Corrosion and Protection, 2014, 34(4): 327 − 332.

[17] 孔德军, 王进春, 叶存冬. X70 高钢级管线钢焊接接头盐雾腐蚀机理 [J]. 焊接学报, 2015, 36(5): 51 − 54.
Kong Dejun, Wang Jinchun, Ye Cundong. Mechanism of salt spray corrosion of X70 high grade pipeline steel welded joints[J]. Transactions of the China Welding Institution, 2015, 36(5): 51 − 54.

[18] 范舟, 刘建仪, 李士伦, 等. X70 管线钢焊接接头组织及其海水腐蚀规律 [J]. 西南石油大学学报 (自然科学版), 2009, 31(5): 171 − 174.
Fan Zhou, Liu Jianyi, Li Shilun, *et al*. Microstructure and seawater corrosion to welding joint of X70 pipeline steel[J]. Journal of Southwest Petroleum University (Science & Technology Edition), 2009, 31(5): 171 − 174.

[19] 刘智勇, 万红霞, 李禅, 等. X65 钢焊接接头在模拟浅表海水和深海环境中的腐蚀行为对比 [J]. 中国腐蚀与防护学报, 2014, 34(4): 321 − 326.
Liu Zhiyong, Wan Hongxia, Li Chan, *et al*. Comparative study on corrosion of X65 pipeline steel welded joint in simulated shallow and deep-sea environment[J]. Journal of Chinese Society for Corrosion and Protection, 2014, 34(4): 321 − 326.

[20] 林鑫, 杜敏, 李成杰, 等. DH36 钢焊接件海水腐蚀行为研究 [J]. 中国海洋大学学报(自然科学版), 2013, 43(3): 70 − 74.
Lin Xin, Du Min, Li Chengjie, *et al*. Study on corrosion in seawater of welded DH36 steel[J]. Periodical of Ocean University of China, 2013, 43(3): 70 − 74.

[21] Liang Ping, Shi Yanhua, Zhang Yunxia, *et al*. Characterization of passive film formed on X80 pipeline steel in sodium bicarbonate solution[J]. Advanced Materials Research, 2013(690−693): 101 − 105.

[22] 李金波, 左剑恶. 温度对 X80 管线钢钝化膜电化学性能的影响 [J]. 中国腐蚀与防护学报, 2009, 29(1): 40 − 43.
Li Jinbo, Zuo Jian’e. Influence of temperature on the electrochemical property of passive film formed on x80 pipeline steel[J]. Journal of Chinese Society for Corrosion and Protection, 2009, 29(1): 40 − 43.

[23] 张忠明, 马莹, 马艳艳, 等. Mg-1Zn-1Mn 合金微弧氧化膜在 SBF 模拟体液中的腐蚀行为 [J]. 材料热处理学报, 2018, 39(5): 108 − 116.
Zhang Zhongming, Ma Ying, Ma Yanyan, *et al*. Corrosion behavior of micro-arc oxidation film of Mg-1Zn-1Mn alloy in SBF simulated body fluid[J]. Transactions of Materials and Heat Treatment, 2018, 39(5): 108 − 116.

[24] Wang Yafei, Cheng Guangxu, Wu Wei, *et al*. Effect of pH and chloride on the micro-mechanism of pitting corrosion for high strength pipeline steel in aerated NaCl solutions[J]. Applied Surface Science, 2015, 349(15): 746 − 756.

[25] 刘智勇, 董超芳, 贾志军, 等. X70 钢在模拟潮湿存储环境中的点蚀行为 [J]. 金属学报, 2011, 47(8): 1009 − 1016.
Liu Zhiyong, Dong Chaofang, Jia Zhijun, *et al*. Pitting corrosion of X70 pipeline steel in the simulated wet storage environment[J]. Acta Metallurgica Sinica, 2011, 47(8): 1009 − 1016.

第一作者:张忠明，博士，教授；主要研究方向为先进材料制备及成形技术；Email：zmzhang@xaut.edu.cn.
通信作者:黄继强，副教授. Email：huangjiqiang@bipt.edu.cn.

（编辑： 郑红）

loses the support of the binder phase and is exposed, peeling off under the continuous attack of erosive sand, forming many small erosion pits. With the increase of the number of hard phases peeling off, small erosion pits gradually develop into large erosion pits, with greater weight loss and poor erosion resistance.

Highlights: (1) The effect of impingement angle on the erosion resistance of supersonic flame sprayed Cr_3C_2-NiCr cermet composite coating was studied.
(2) The effect of impingement angle on the impact resistance of the coating was explained from the perspective of erosion mechanism.

Key words: HVOF; Cr_3C_2-NiCr coating; impingement angle; erosion mechanism

Effect of heat treatment on microstructure and high temperature properties of IC10 superalloy TLP diffusion welding under 80 μm gap LI Qi, LIU Fengmei, YUE Xiong, XIONG Min, YI Yaoyong, GAO Haitao (China-Ukraine Institute of Welding, Guangdong Academy of Sciences, Guangdong Academy of Sciences Guangdong Provincial Key Laboratory of Advanced Welding Technology, Guangzhou, 510650, China). pp 36-44

Abstract: The IC10 superalloy with 80 μm gap was welded by TLP diffusion welding. The microstructure, morphology, modulus of elasticity, microhardness, high temperature tensile strength, high temperature durability and fracture morphology before and after heat treatment of IC10 joints were tested by using scanning electron microscopy (SEM/EDS), nano-indenter and high-temperature tensile testing machine. The results showed that when SBM-3 was used as the intermediate solder and the gap size of the weld was 80 μm, under the welding process conditions of 1 250 ℃, 5 MPa, and 6 h, the morphology and base composition of the weld seam and the base metal were similar. After heat treatment, the tensile strength was 268 MPa, which higher than 97.5% of base metal (275 MPa) at the test temperature of 1 100 ℃. The high temperature durability of the IC10 joints were tested, the creep time of the joints was more than 117 h under the condition of the temperature of 1 100 ℃ and the stress of 36 MPa, which was higher than 90% of the base material. In the joint structure, a larger volume of $\gamma + \gamma'$ phase existed in the weld, and the joint structure transitioned smoothly from the base material to the welded joints. In high-temperature tensile and high-temperature durability tests, cracks started to expand from at the edge of the borides and carbides as well as the edge of the $\gamma + \gamma'$ eutectic. Heat treatment increased the elastic modulus of the base material while reduced the elastic modulus of the weld. The reduction of the joint elastic modulus improves the high-temperature mechanical strength of the TLP diffusion welded joints.

Highlights: (1) A new Ni-based intermediate layer powder was prepared and applied to IC10 superalloy TLP diffusion welding with the gap of 80 μm.
(2) The influence of heat treatment on the microstructure and high temperature mechanical properties of the IC10 joints were discussed. The high temperature mechanical properties of the IC10 joints after heat treatment were excellent.

Key words: IC10 superalloy; TLP diffusion welding; microstructure; high temperature tensile; high temperature durability

Corrosion behavior of X65 pipeline steel welded joints by hyperbaric GMAW in simulated seawater ZHANG Zhongming[1,2], XUE Long[2], LI Qilong[1], HUANG Jiqiang[2], XU Chunjie[1] (1. Xi 'an University of Technology, Xi 'an, 710048, China; 2. Opto-mechatronic Equipment Technology Beijing Area Major Laboratory, Beijing Institute of Petrochemical Technology, Beijing, 102617, China). pp 45-50

Abstract: Hyperbaric dry GMAW is widely employed commercially in the fabrication and maintenance of submarine oil and gas pipelines. The corrosion behaviors of welded joint in seawater are therefore of utmost importance in security operation of the pipelines. The corrosion performance and mechanism of X65 pipeline steel welded joints by hyperbaric

GMAW under different ambient pressures (0. 1, 0. 3, 0. 5 MPa) were studied by polarization curves and immersion simulation experiments in artificial seawater. It was found that compared with the welding base metal and welded zone, the corrosion resistance of heat affected zone is the worst, and the ambient pressure has little effect on the corrosion resistance of the welded joint. Corrosion morphology and corrosion product shows that pitting corrosion is the main corrosion form for the welded joints, and serious local pitting corrosion occurs at the late immersion stage. The corrosion product is composed of FeOOH, Fe_2O_3 and Fe_3O_4. The corrosion product on the surface of the welded joints can mitigate the corrosion at the initial immersion stage. With prolonged immersion durations, the compactness of the corrosion products layer reduces, the metal under the layer is vulnerable to the corrosion by Cl^-, and thus the local pitting corrosion process is promoted.

Highlights: (1) This paper describes corrosion performance and behavior of X65 pipeline steel welded joints by hyperbaric GMAW in simulated seawater. It was found that the corrosion resistance of heat affected zone is the worst, and the ambient pressure has little effect on the corrosion resistance of the welded joint.
(2) The study reveals corrosion mechanism of the welded joint and role of corrosion products. It was found that pitting corrosion is the main corrosion form.

Key words: X65 pipeline steel; hyperbaric welding; gas metal arc welding; corrosion resistance

Effect mechanism of Ni-P coating on the structure and properties of Cu/Al joints HUANG Junlan[1], LONG Weimin[1], ZHONG Sujuan[1], GENG Jinfeng[2], DING Tianran[1], QIN Jian[1] (1. State Key Laboratory of Advanced Brazing Filler Metals and Technology, Zhengzhou Research Institute of Mechanical Engineering Co., Ltd., Zhengzhou, 450001, China; 2. State Grid Henan Electric Power Research Institute, Zhengzhou, 450052, China). pp 51-56,70

Abstract: To investigate the influence of Ni-P coating on the interfacial reaction of Cu/Al dissimilar metal brazing, two brazing filler metals, Zn98Al and BAl67CuSi, were first used to braze 3003 aluminum alloy and T2 copper with or without Ni-P coating. Four different brazing joints were obtained. The Cu side interfacial microstructure, joint shear strength, joint fracture morphology, joint microhardness and joint bending morphology were systematically studied. Additionally, the joints without Ni-P coating were also used for comparison. The results showed that the interfacial structure of the Cu/Zn98Al/Al brazed joint was Cu/diffusion layer+8. 8 μm thickness $Cu_{3.2}Zn_{4.2}Al_{0.7}$. After the preparation of the Ni-P coating on the T2 copper surface, the interfacial structure transformed into Ni-P coating+1. 5 μm thickness Al_3Ni, which leaded to the higher strength and toughness. However, the interfacial structure of the Cu/BAl67CuSi/Al brazed joint changed from diffusion layer+15 μm thickness $CuAl_2$ to Ni-P coating+1. 8 μm thickness Cu_3NiAl_6, which leaded to the higher toughness but the lower strength. The effect mechanism of Ni-P coating on the interfacial reaction of Cu/Al joint was clarified. The mechanical properties test results were consistent with the microstructure transition of the Cu side interface of the joint. Finally, the interfacial reaction model of the Cu/Al joint was established, and the influence mechanism of Ni-P coating on the interfacial structure and mechanical properties of the Cu/Al joint was illustrated.

Highlights: (1) The indirect brazing method of 3003 aluminum alloy and T2 with Ni-P coating was designed;
(2) By improving the brittleness of Cu/Al joints, the Cu/Al joints were obtained with high strength and toughness.

Key words: Ni-P coating; Cu/Al joint; interface structure; strength; toughness

Effect of Zn on the shear properties of Sn0.5Ag0.7Cu/Cu joints and the microstructure of aging joints ZHANG Min, ZHU Ziyue, XU Huanrui, WANG Gang, DU Mingke, WANG Boyu (Xi 'an University of Technology, Xi 'an, 710048, China). pp 57-64